

# Crustal density structure in the Spanish Central System derived from gravity data analysis (Central Spain)

D. Gómez-Ortiz<sup>a,b,\*,1</sup>, R. Tejero-López<sup>b,1</sup>, R. Babín-Vich<sup>b,1</sup>, A. Rivas-Ponce<sup>b,1</sup>

<sup>a</sup>ESCET-Área de Geología, Universidad Rey Juan Carlos, C/Tulipán s/n, Móstoles, 28933 Madrid, Spain

<sup>b</sup>Depto. Geodinámica, Facultad de CC. Geológicas, Universidad Complutense de Madrid, C/Jose Antonio Novais s/n, 28040 Madrid, Spain

---

## Abstract

Shallow and deep sources generate a gravity low in the central Iberian Peninsula. Long-wavelength shallow sources are two continental sedimentary basins, the Duero and the Tajo Basins, separated by a narrow mountainous chain called the Spanish Central System. To investigate the crustal density structure, a multitaper spectral analysis of gravity data was applied. To minimise biases due to misleading shallow and deep anomaly sources of similar wavelength, first an estimation of gravity anomaly due to Cenozoic sedimentary infill was made. Power spectral analysis indicates two crustal discontinuities at mean depths of  $31.1 \pm 3.6$  and  $11.6 \pm 0.2$  km, respectively. Comparisons with seismic data reveal that the shallow density discontinuity is related to the upper crust lower limit and the deeper source corresponds to the Moho discontinuity. A 3D-depth model for the Moho was obtained by inverse modelling of regional gravity anomalies in the Fourier domain. The Moho depth varies between a mean depth of 31 km and 34 km. Maximum depth is located in a NW–SE trough. Gravity modelling points to lateral density variations in the upper crust. The Central System structure is described as a crustal block uplifted by NE–SW reverse faults. The formation of the system involves displacement along an intracrustal detachment in the middle crust. This detachment would split into several high-angle reverse faults verging both NW and SE. The direction of transport is northwards, the detachment probably being rooted at the Moho.

*Keywords:* Gravity anomaly; Density crust structure; Moho undulations; Spanish Central System

---

---

\* Corresponding author. ESCET-Área de Geología, Universidad Rey Juan Carlos, C/Tulipán s/n, Móstoles, 28933 Madrid, Spain. Fax: +34 91 664 74 90.

E-mail addresses: david.gomez@urjc.es (D. Gómez-Ortiz), rosatej@geo.ucm.es (R. Tejero-López), rosbabin@geo.ucm.es (R. Babín-Vich), pcarivas@geo.ucm.es (A. Rivas-Ponce).

<sup>1</sup> Fax: +34 91 394 46 31.

## 1. Introduction

Compressional field stress due to convergence of the African and European Plates deformed the Iberian Plate lithosphere, giving rise to intraplate mountain ranges and continental sedimentary basins (Fig. 1). One of these intraplate mountain ranges is the Central

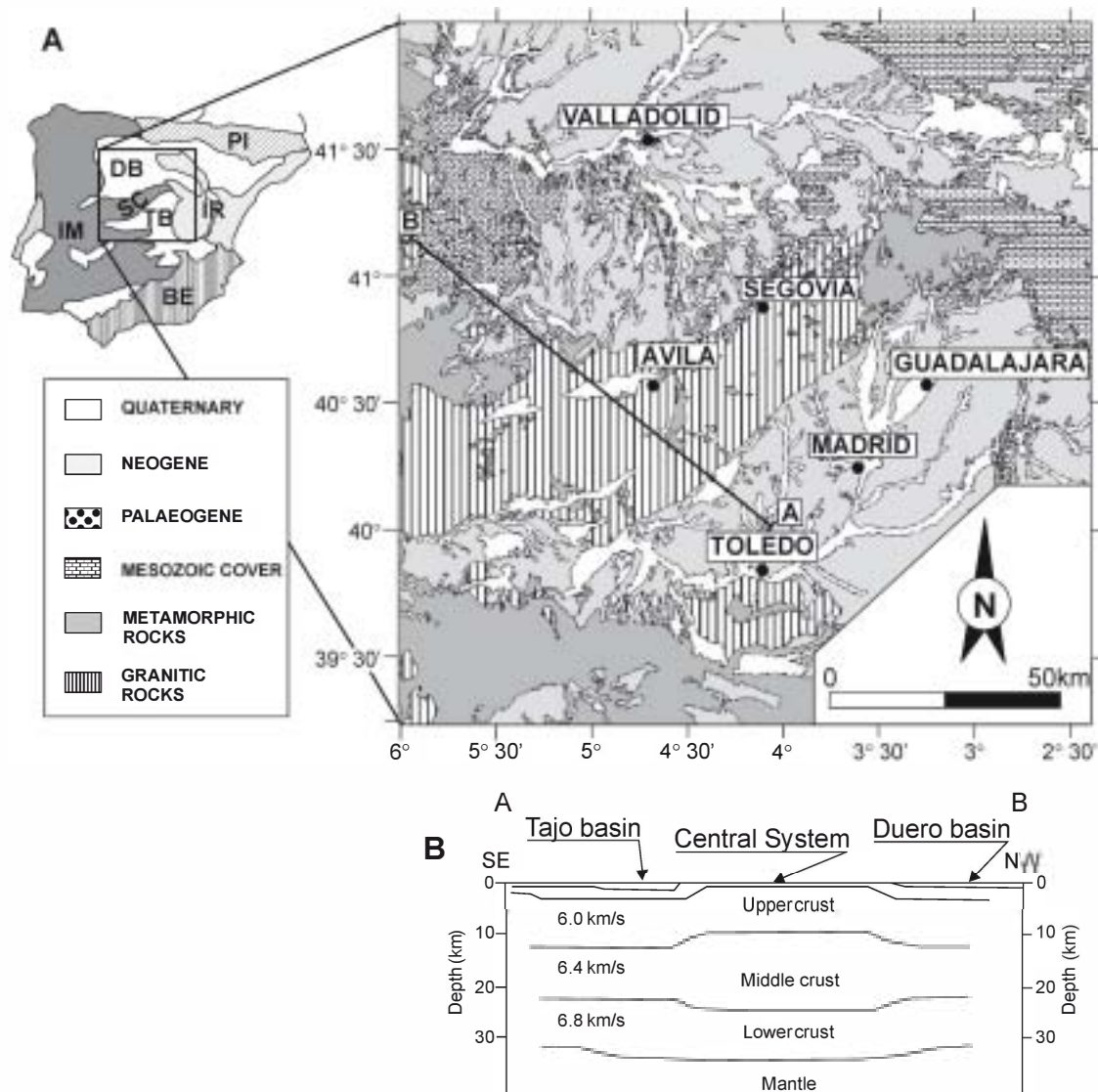


Fig. 1. (A) Main tectonic units of the Iberian Peninsula and geological map of the study area. SC: Spanish Central System; IR: Iberian Range; DB: Duero basin; TB: Tajo Basin; PI: Pyrenees; IM: Iberian Massif; BE: Betics. Geographical coordinates. A–B represents the location of the refraction seismic profile described in the text. (B) Refraction seismic profile (from [Suriñach and Vegas, 1988](#)). crustal layers, together with the P-wave velocities, is shown.

System, which is comprised of an uplifted crustal block bounded by two reverse faults separating it from the Tajo and the Duero basins. Basin depocentres occur close to the chain borders. Here, Cenozoic infill can reach 3000 m ([Aeroservice, 1967](#); [Querol, 1989](#)). Seismic data point to the existence of a thicker crust under the central part of the Iberian Peninsula, lowering the Moho from 30 km to 34 km under the

Central System ([Suriñach and Vegas, 1988](#); [ILIHA, 1993](#)). The area is characterized by a long-wavelength gravity low ([Mezcua et al., 1996](#)) and gravity studies have related it to the Cenozoic infill of basins and to a crust thickening of up to 2 km ([Tejero et al., 1996](#); [Gómez Ortiz, 2001](#)).

In this paper, multitaper spectral analysis of gravity data is used to investigate crustal density

structure in the central part of the Iberian Peninsula. As pointed out by Chakraborty and Agarwal (1992), the filtering technique based on regional-residual separation through the spectral analysis of gravity data is difficult when both shallow and deep anomaly sources have similar wavelengths. It can be argued that the combined effects of gravity anomalies due to sedimentary infilling of the Duero and Tajo basins could affect the amplitude of the anomaly associated with the gravity effect of suspected deep sources, such as the Moho. To avoid this, first the gravity anomaly associated with the Cenozoic sedimentary basins was computed and then this effect was subtracted from the observed gravity map. Published isopach maps, rock sample density measurements and density-logs provided a data set used to calculate this gravity effect. This method let us accurately discriminate between residual and regional sources. The inversion of gravity data has revealed a crustal thickening in the central part of the study zone. Besides the spectral analysis of gravity data, gravity modelling results show the density heterogeneities within the crust.

## 2. Geological setting

The present-day physiographic and tectonic configuration of the intraplate Iberian domain developed in the Cenozoic. Commencing in Permian times and continuing through the Mesozoic, subsidence and rifting occurred along a NW–SE trending trough, the Iberian Basin. NW–SE to WNW–ESE structures controlled Iberian Basin geometry during extensional deformation events associated with Mesozoic rifting in the NW margin of the basin. Collision of the European and Iberian Plates caused the tectonic inversion of the Iberian Basin, giving rise to the Iberian Range (Fig. 1A). During the Neogene, collision of the south-eastern margin of the Iberian and African Plates triggered compressive deformations in the south and centre of the plate, building up the Central System (centre) and Betic Cordillera (south) (e.g., Vegas et al., 1990; De Vicente et al., 1996a,b).

The exposed bedrock of the Central System (Fig. 1A) is comprised of low and high grade metamorphic rocks and granitoids from the Variscan base-

ment. The Central System chain has been described as an uplifted crustal block (Vegas et al., 1990; Capote et al., 1990; De Vicente et al., 1996a,b) bounded by two main reverse faults trending NE–SW. The range is characterized by E–W to NE–SW alignments of “sierras” (uplifted blocks) and topographic depressions (mainly small Cenozoic sedimentary basins). Mesozoic cover is mainly preserved in the easternmost part of the study area and the interior of some tectonic depressions. NE–SW folds, thrust and reverse faults deform the cover as well as the basement. To the east of the study area, outcrops the westernmost Iberian Range. It consists of a NW–SE intraplate mountain range arising from Mesozoic basin inversion. The Iberian Range bounds the eastern margins of the Duero and the Tajo Basins. Palaeogene/Neogene basin infill indicates that alpine deformation started in Eocene times, and was the main range building event in the Middle to Upper Miocene (De Vicente et al., 1996b). The sedimentary basins are the Duero Basin to the north and the Tajo Basin to the south. Palaeogene sediments overlay a thin Mesozoic cover, which may even be absent in the west. Basin depocentres appear close to the chain borders. The eastern part of the Duero Basin consists of a small depression, infilled with up to 3500 m of Cenozoic sediments, denoted the Almazan Basin. Magnetic and seismic reflection profiles indicate Cenozoic sedimentary thicknesses of up to 3 km (Querol, 1989; Aeroservice, 1967; Bond, 1996; Maestro, 1999; Rey Moral, 2001).

Refraction seismic studies in the central Iberian Peninsula show that the crust is comprised of three layers (e.g., Banda et al., 1981; Suriñach and Vegas, 1988; ILHA, 1993): a 11 to 14 km thick upper crust, a 10 to 14 km thick middle crust and a 9 km thick lower crust (Fig. 1B). Mean crustal thickness is 31 km although a seismic model transverse to the Central System reveals that the crust thickens to attain a thickness of 34 km (Suriñach and Vegas, 1988, Fig. 1B). Tectonic interpretations of Central System formation have considered two models: crustal thrusting (Warburton and Alvarez, 1989; Ribeiro et al., 1990; Tejero et al., 1996) or a distributed deformation accompanied by homogeneous crustal thickening of the lower crust (Vegas et al., 1990).

### 3. Bouguer anomaly map of the central Iberian Peninsula

Two sets of gravity data were used in this study. The first set corresponds to our own data derived from 2892 gravity stations covering an area of about 23,657 km<sup>2</sup> in Central Spain (Fig. 2, inset). All gravity measurements were corrected for Earth-tide effects, and free-air and Bouguer reductions were also applied. Terrain correction up to 166.7 km was also undertaken. In addition, we used data from the Bouguer anomaly map of the Iberian Peninsula (Mezcua et al., 1996) to extend our study area to a size of 500 km × 500 km. A comparison of 469 duplicate gravity measurements

for the two data sets revealed a root mean square error of  $\pm 0.88$  mGal. This is acceptable for a regional study and indicates the different data sets can be used together. The density value used in the Bouguer reduction was 2670 kg/m<sup>3</sup>. Kriging was used to interpolate the Bouguer anomaly values. The final grid size was 101 rows by 101 columns, with a spacing of 5 km and a total length of 500 km both in *x* and *y* directions.

The Bouguer anomaly map presents a long-wavelength gravity low which reaches a minimum value up of -140 mGal. Some superimposed gravity lows are associated with Cenozoic basin depocentres (Querol, 1989; Aereservice, 1967) (Fig. 2). Among

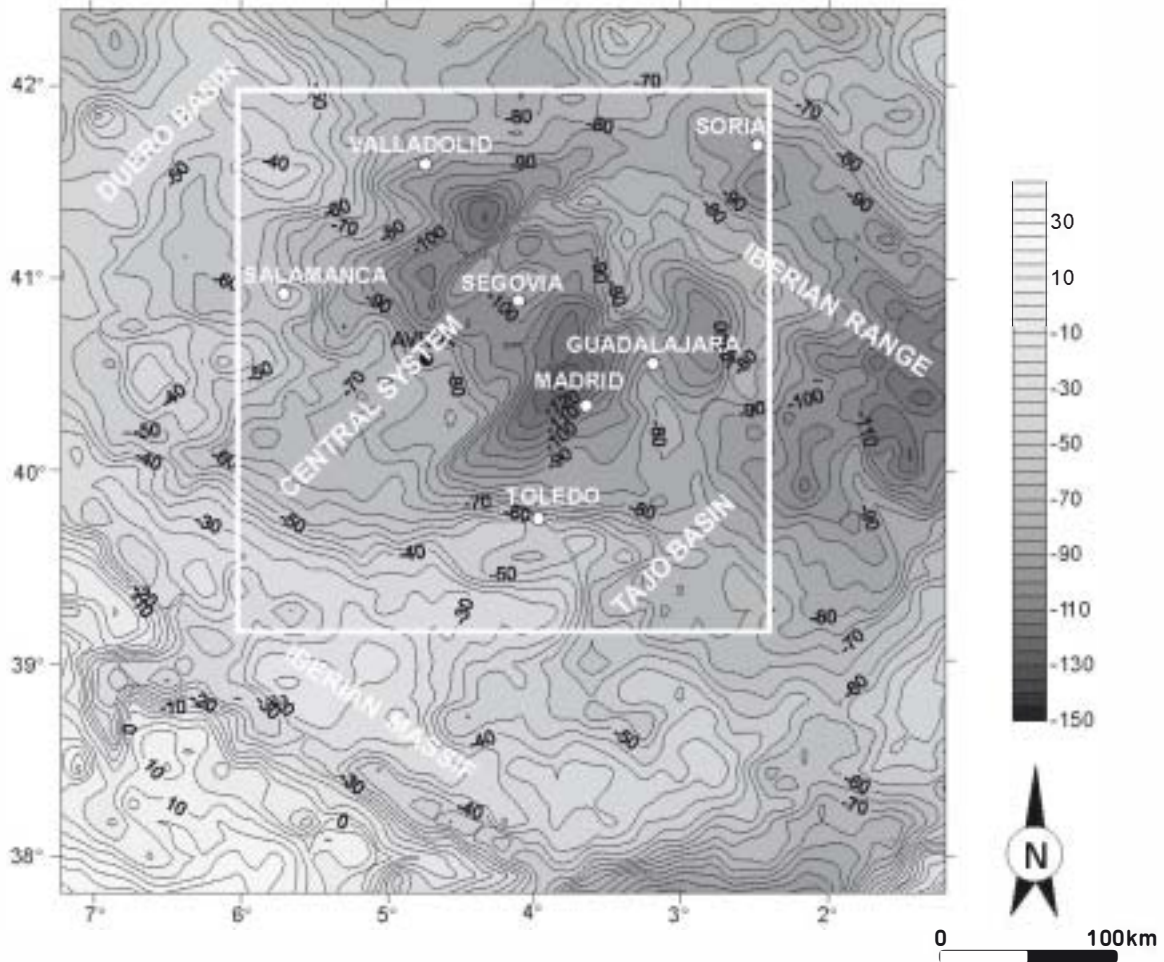


Fig. 2. Bouguer anomaly map of Central Spain. Contour interval 5 mGal. Geographical coordinates. The outlined area is the zone represented in Fig. 1, where gravity modelling was performed.



the most striking features of the map are the strong NE-SW gradients that bound the relative gravity lows related to basin depocentres. These are associated with the reverse faults that bound the Central System and basins. Between the two gravity gradients, a relative gravity high representing the Central System is observed. Three distinctive areas can be defined in this gravity high. The easternmost part is characterized by N-S and E-W trending gravity highs associated with outcrops of low-grade metamorphic rocks. The boundary between this area and the central zone corresponds to a strong gravity gradient of N-S orientation. More negative values characterize this area, where granite bodies and high-grade metamorphic rocks outcrop. To the west, a new gravity gradient trending NW-SE corresponds to the transition to the westernmost area, where the gravity values became less negative,

reaching about  $-80$  mGal. This zone is associated with large granite bodies, which represent the main lithology of the westernmost part of the Central System.

A spectral analysis was conducted to evaluate regional and residual gravity sources. Bearing in mind that sedimentary basin infilling can generate a long wavelength Bouguer anomaly, we first estimated the Bouguer anomaly associated with this sedimentary infilling and then removed this effect from the observed Bouguer gravity map.

#### 4. Gravity effect due to Cenozoic basin sedimentary infilling

Several two-dimensional and three-dimensional methods have been proposed to estimate the gravity

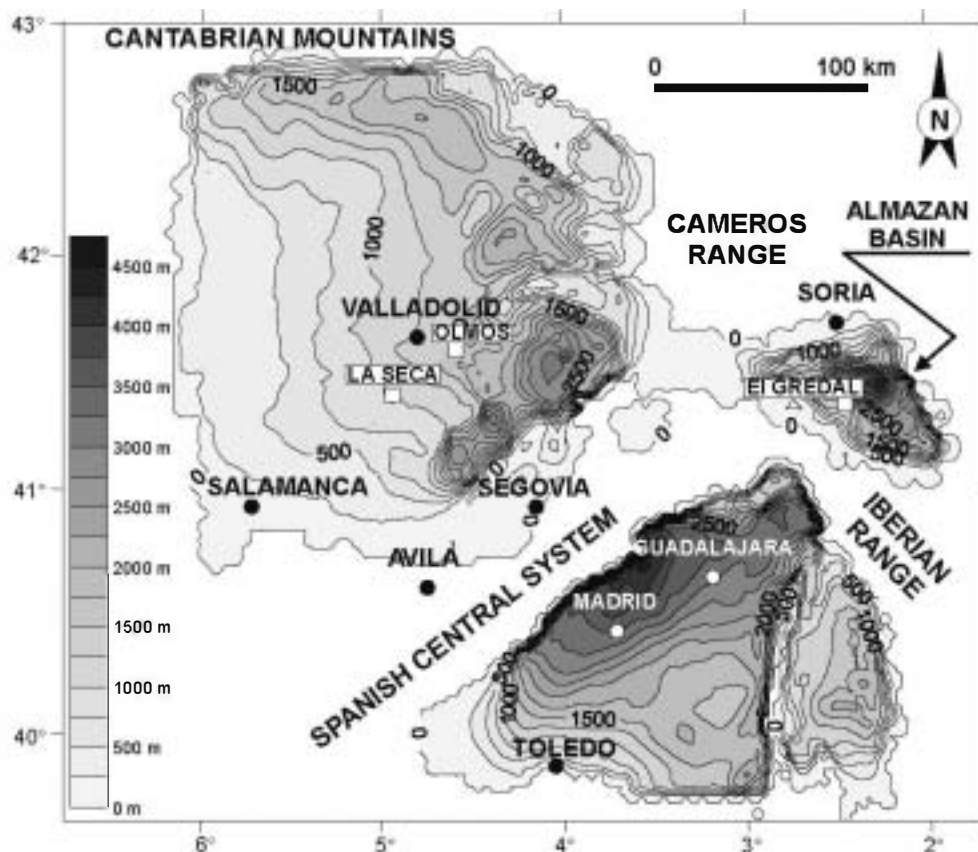


Fig. 3. Isopach map for the bottom of the Tertiary obtained for the Duero and Almazan, and Tajo Cenozoic basins. Contour interval 250 m. Geographical coordinates.

anomaly associated with the sedimentary infilling of basins (Bott, 1960; Cordell, 1973; Granser, 1987; Chai and Hinze, 1988; Martin-Atienza and Garcia-Abdeslem, 1999, among others). Here, the GRAV3D-BASE forward modelling technique (Chakravarthi et al., 2002) was used to compute the gravity anomaly associated with the Cenozoic basins of the study area. Density-depth variation was calculated by the parabolic function (Chakravarthi and Rao, 1993):

$$\Delta\rho(z) = \frac{\Delta\rho_0^3}{(\Delta\rho_0 - \alpha z)^2} \quad (1)$$

where  $\Delta\rho$  is the density contrast,  $z$  is the depth,  $\Delta\rho_0$  is the density contrast at the surface and  $\alpha$  is a constant expressed in  $\text{kg/m}^3/\text{km}$  that can be determined by fitting Eq. (1) to known density contrast-depth data for sedimentary rocks. The gravity anomaly is calculated for a 3D prism at each node of the isopach map of the basin, and then the gravity anomaly at any point is determined by adding the individual effect of each prism.

#### 4.1. Application to the Duero and Tajo Basins

Two types of information are needed to determine the gravity anomaly associated with a sedimentary basin: (1) an isopach map and (2) the variation of the density contrast basement-sediments at depth.

We compiled published isopach maps of the Duero and Tajo basins (Blanco and Merten, 1974; Querol, 1989; Muñoz Martín, 1997; Maestro, 1999; Rey Moral, 2001). Fig. 3 shows the isopach maps representing the thickness of the Cenozoic sedimentary Duero and Tajo basins, and the positions of the three wells used to compute the density-depth variation curve. Fig. 4 shows the lithologies and density-logs for each well. As can be seen in Fig. 3, sedimentary thickness increases from west to east in the Duero basin, with depocentres bordering the Cantabrian Mountains, Cameros Range and the northern limit of the Central System, where maximum thicknesses of 3000 m are reached (Aeroservice, 1967; Blanco and Merten, 1974; IGME, 1987; ITGE, 1990). The Almazan basin, which is connected to the Duero basin

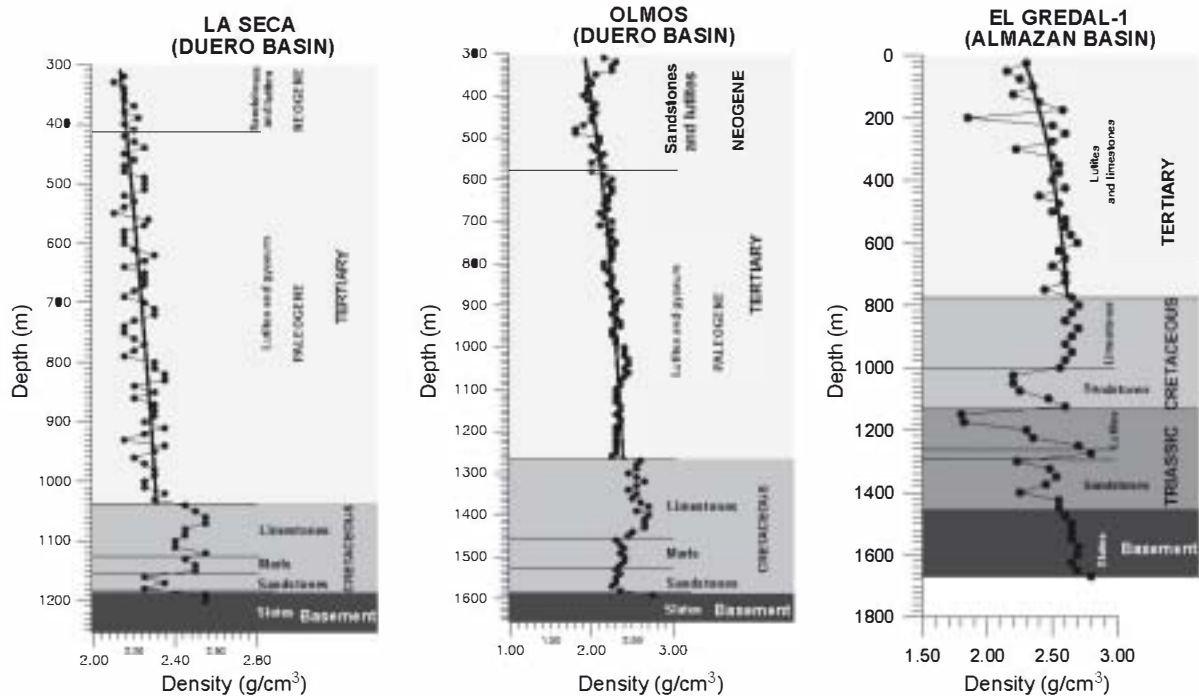


Fig. 4. Density-logs and lithological units obtained from the three wells available in the study area. The density-depth parabolic function is also indicated for each case.

via its westernmost edge, attains a sedimentary thickness of up to 4000 m (ITGE, 1990; Bond, 1996; Maestro, 1999; Rey Moral, 2001) including Upper Cretaceous, Palaeogene and Neogene sediments. On the other hand, the Tajo basin (Fig. 3) shows a sedimentary thickness increasing from south to north, with its depocentre located at the southern border of the Central System, where thicknesses peak at 3500 m (Querol, 1989).

The density contrast between basement and sediments was estimated from density-log data from wells in the Duero Basin (ITGE, 1990; SHELL, 1983). No density-logs are available for the Tajo basin. Fig. 4 shows the lithological units represented in the wells (La Seca, Olmos and El Gredal-1). The parabolic fit that best describes the density-depth curve obtained

from the density-log data gives values of  $\Delta\rho_0 = -600$  kg/m<sup>3</sup> and  $\alpha = 155$  kg/m<sup>3</sup>/km for the La Seca well, and  $\Delta\rho_0 = -980$  kg/m<sup>3</sup> and  $\alpha = 615$  kg/m<sup>3</sup>/km for the Olmos well and of  $\Delta\rho_0 = -360$  kg/m<sup>3</sup> and  $\alpha = 154$  kg/m<sup>3</sup>/km for the El Gredal-1 well. For gravity anomaly estimates, we adopted mean values of  $\Delta\rho_0 = -600$  kg/m<sup>3</sup> and  $\alpha = 155$  kg/m<sup>3</sup>/km to determine the gravity effect of the Duero and Almazan basins. Given that, as mentioned above, there is no density-log for the Tajo basin yet this basin has a similar sedimentary record, we also used these values for the Tajo basin.

Fig. 5 provides the gravity anomaly computed for each basin using the density-depth values estimated and the GRAV3DBASE forward modelling technique. The Duero basin shows a maximum gravity anomaly of -32 mGal, the Almazan basin one of -34 mGal

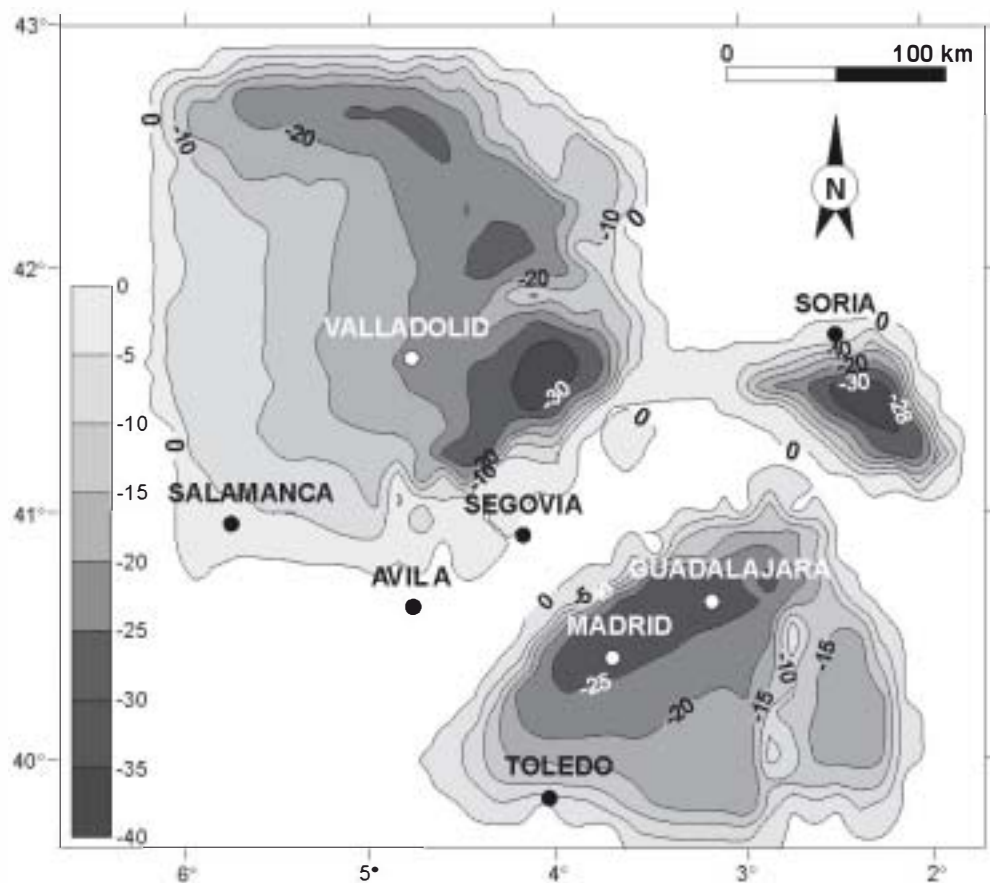


Fig. 5. Theoretical gravity map due to the sedimentary infill obtained for the Duero and Almazan, and Tajo Cenozoic basins. Contour interval 5 mGal. Geographical coordinates.

and the Tajo basin  $-28$  mGal. These maps were then subtracted from the observed Bouguer anomaly map to obtain a residual gravity map (Fig. 6), reflecting only the crustal structure of Central Spain. The new map obtained has values ranging from  $+20$  mGal to  $-115$  mGal, with a relative gravity low in the centre of the study area (Central System) and relative gravity highs close to the northern and south-western edges. The two strong gravity gradients that previously defined the limits of the Central System with the sedimentary basins are now only discrete, and the relative gravity highs and lows of small wavelength appearing in this map are now assumed to reflect the heterogeneous nature of the basement in this area.

## 5. Estimating mean depths of main crustal density discontinuities

Several spectral techniques can be used to estimate the power spectrum of a gravity anomaly. Herein, we used the multitaper method that provides an optimal spectrum estimate by minimising spectral leakage, while reducing the variance of the estimate by averaging orthogonal eigenspectrum estimates (Lees and Park, 1995). In order to do this, ideal data windows have to be obtained and these are given by prolate spheroidal sequences (Slepian, 1978). Due to the two-dimensional character of the data set analysed, radial averaging of the power spectrum was performed to

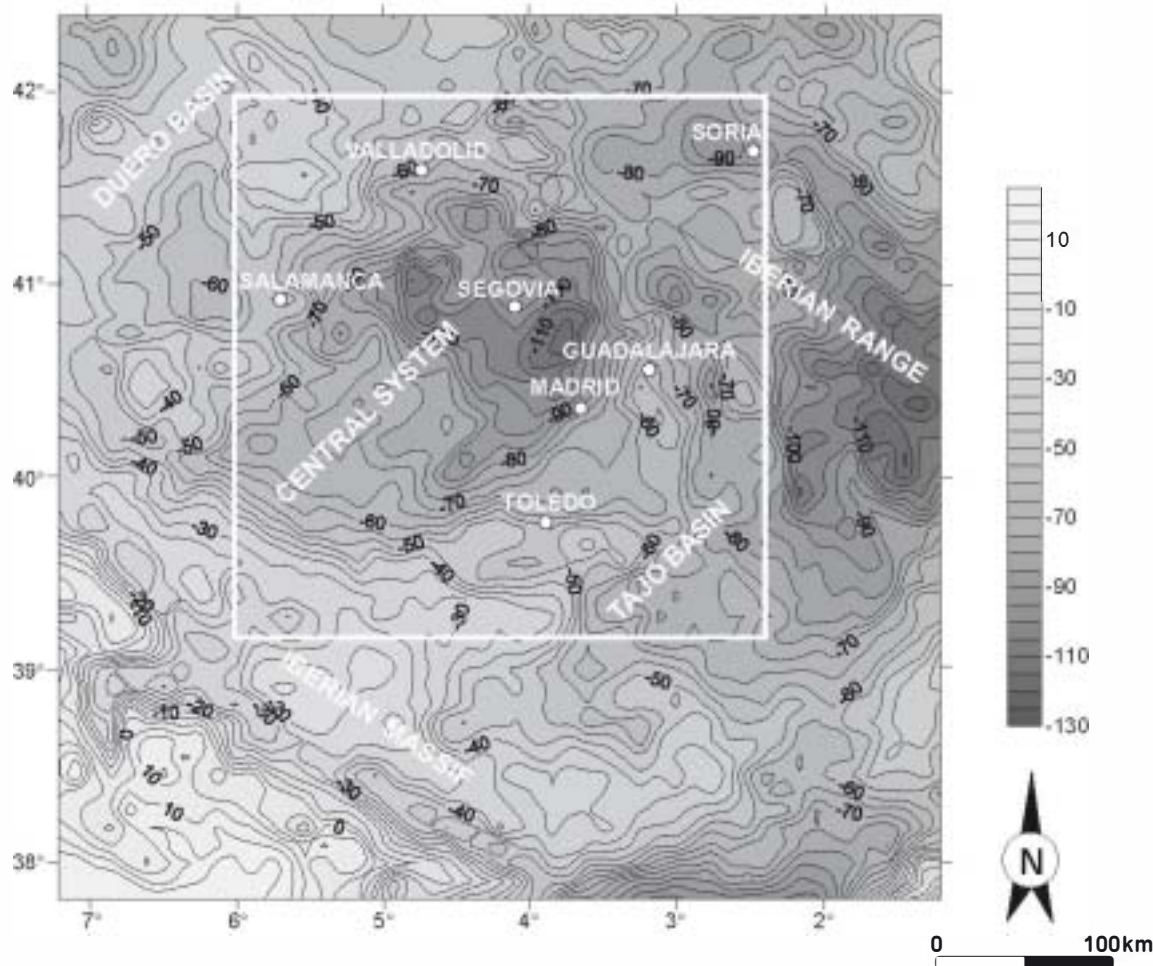


Fig. 6. Bouguer anomaly map of Central Spain obtained by subtracting the theoretical anomaly maps in Fig. 5 from the observed anomaly map in Fig. 2. Contour interval 5 mGal. Geographical coordinates. The outlined area is the same as in Fig. 2.



obtain a one-dimensional representation. The process involves averaging of the power spectrum values by means of concentric circles of different radius, expressed as frequency values, sharing a common origin (Mishra and Naidu, 1974; Dimitriadis et al., 1987; Tselentis et al., 1988).

Fig. 7 is a graph of the natural logarithm of the gravity power spectrum versus the frequency for the study area (Fig. 6) after subtracting the gravity effect of the sedimentary basins. Three frequency domains are defined in this figure. The first one, domain A, corresponds to a frequency of up to  $0.03 \text{ km}^{-1}$  and the mean depth of the source, as determined from the slope of the linear segment fitted to the data is  $31.1 \pm 3.6 \text{ km}$ . The second one, domain B, corresponds to a frequency ranging from  $0.03$  to  $0.09 \text{ km}^{-1}$ , and the mean depth of the causal source is  $11.6 \pm 0.2 \text{ km}$ . The third domain comprises the final part of the power spectrum and is considered white noise. From seismic studies, we can link the

deeper level to Moho discontinuity and the shallower level to the base of the upper crust (Banda et al., 1981; Surinach and Vegas, 1988; ILHA, 1993).

In Fig. 7, we have also represented the natural logarithm of the observed gravity power spectrum for comparison. It can be seen that, whereas the linear segments fitted to the white noise and residual source are nearly identical to the ones from the Bouguer anomaly without the gravity effect of the basins, the regional source is poorly determined if the gravity effect of the basins is not subtracted. The power spectrum of the regional source shows an oscillating behaviour that defines a linear segment with a lower slope (a lower mean depth) and a poor correlation. When the gravity effect of the basins is subtracted, the regional source shows a better marked linear rate of decay, so the mean depth of the regional source is better defined than in the other case.

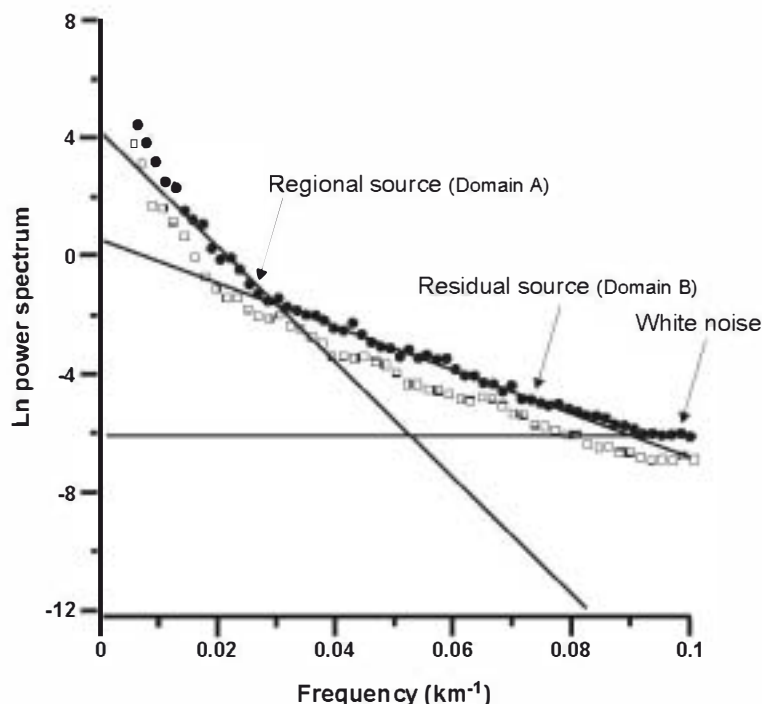


Fig. 7. Graph representing the natural logarithm of the radial gravity power spectrum versus the frequency for the Bouguer anomaly map without the gravity effect of the sedimentary basins (black circles). Three domains have been recognised, a regional source (A), a residual source (B) and a white noise. The radial gravity power spectrum for the observed Bouguer anomaly has been represented for comparison (open squares).

## 6. Regional and residual gravity maps

Having established the main sources contributing to the gravity anomalies of the study area and their mean depths, we now need to define a filter to isolate the anomalies associated with each source. There are several examples of the application of filtering procedures in the literature (Syberg, 1972; Spector and Grant, 1970; Gupta and Ramani, 1980; Lefort and Agarwal, 2002, among others). In this work, a cosine roll-off type filter was used. This is a spectral domain pass filter that retains long-wavelength components of observed data using taper with a smooth cosine curve in roll-off range. High and low frequency (short- and long-wavelength) cut-offs for the roll-off range and a degree for the cosine function need to be specified: the higher the degree, the steeper the transition between passed and rejected portions of the data spectrum. Unlike conventional pass filters, the cosine roll-off filter has strongly reduced null ringing effects. Based on the analysis of the radial power spectrum, the frequency cut-offs adopted here for the roll-off range were  $0.02 \text{ km}^{-1}$  and  $0.03 \text{ km}^{-1}$ , and the degree of the cosine function was set at 2, which is a suitable value for reducing ringing effects.

Fig. 8A and B, respectively provide the regional and residual gravity maps obtained by applying this filter to the Fourier transform of the demeaned and detrended observed gravity map, after conversion to the spatial domain taking the inverse Fourier transform. The gravity map for the regional source (Fig. 8A) shows an anomaly of +20 to  $-80 \text{ mGal}$ , characterized by a WNW–ESE relative gravity low.

The residual gravity map (Fig. 8B) is the result of subtracting the regional gravity map from the observed Bouguer anomaly map. The gravity anomaly ranges from +15 to  $-40 \text{ mGal}$ . The distribution of anomalies is similar to the observed Bouguer anomaly map, and their main features are the strong gradients associated with the main boundary faults that limit the Central System both to the north and south. Maximum gravity lows are related to the three Cenozoic basins in the study area: the Duero, Almazan and Tajo basins. Several minor gravity highs and lows of predominant NW–SE orientation also appear. Most of these show good correlation with local geological features such as granite bodies, metamorphic outcrops and main faults.

## 7. 3D Moho depth model

Once the regional anomaly (Fig. 8A) has been isolated, it is inverted to obtain the geometry of the density interface causing the anomaly. The inversion method used here is that proposed by Oldenburg (1974), in which the topography of a density interface generating a certain gravity anomaly is estimated using the equation described by Parker (1973). To do this, we need to know both the mean depth of the interface and the density contrast between the bodies separated by this interface. According to Parker (1973), the Fourier transform of the gravity anomaly and the sum of Fourier transforms of the topography causing such a gravity anomaly are related. Using this relationship, Oldenburg (1974) proposed an iterative method in which the topography related to the gravity anomaly is estimated for the first term of the Fourier series, and the resulting topography is then used to calculate the gravity anomaly for the next term. The iterative process finishes after a certain number of iterations have been completed or when the difference between two successive approximations of the topography is lower than a previously established error level. The process is convergent if the depth to the interface is greater than 0 (i.e., it does not intercept the topography) and the amplitude of the interface relief is lower than the mean depth of the interface.

As the inversion operation is unstable at high frequencies, a high-cut filter is needed to ensure convergence. The filter used was that proposed by Oldenburg (1974): a Hamming window with a value of 1 for low frequencies (WH), 0 for high frequencies (SH) and

$$1/2 \left[ 1 + \cos \left( \frac{k - 2\pi WH}{2(SH - WH)} \right) \right] \quad (2)$$

for intermediate frequencies,  $k$  being the wavenumber (i.e.,  $2\pi/\text{wavelength}$ ). After the process is completed, it is desirable to compute the gravity anomaly produced by the calculated topography. This anomaly should be very similar to the one used as the input in the first step of the inversion procedure. Oldenburg (1974) remarks that this method can be extended to the three-dimensional case when the gravity anomaly is measured over a plane. This is not the case in the study area, where the gravity stations are not located

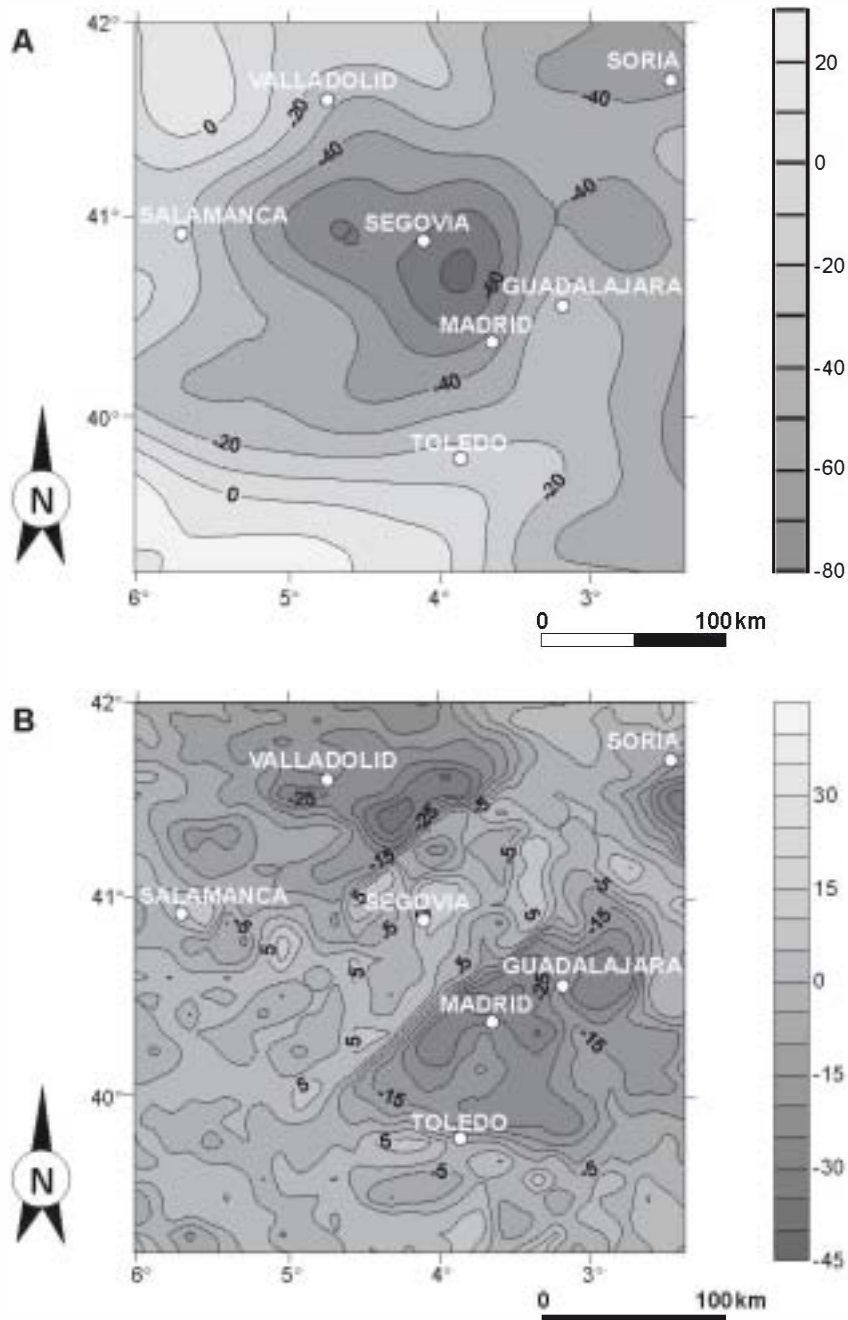


Fig. 8. (A) Regional gravity map obtained by applying a cosine roll-off filter defined from the data derived from the spectral analysis to the Bouguer anomaly map in Fig. 5. (B) Residual gravity map obtained by subtracting the regional gravity map obtained from the observed gravity map in Fig. 5. Both maps: contour interval 5 mGal. Geographical coordinates.

at a constant elevation and this can pose some additional indetermination in the Moho topography computation. However, the differences may be only of a few mGal and we infer that this cannot invalidate the results.

The results obtained in our spectral analysis enabled us to use the previously established value of 31.1 km as the mean reference depth. Crust layer densities were estimated using the P-wave velocity–density empirical relationship applying the Christensen and Mooney (1995) algorithm. Table 1 provides the published crust layer velocities used and estimated densities for the layers. Fig. 9 shows the Moho topography of the area examined. We used a density contrast between crust and mantle of 400 kg/m<sup>3</sup>. The residual error between the observed regional gravity map and the theoretical value computed from the Moho topography was  $\pm 10$  mGal.

The Moho topography shows a NW–SE depression at the point where a depth of up to 34 km is reached. The 31 km contour level encloses this depression, describing a trough that runs in a NE–SW direction roughly parallel to the Central System. Crust thickening is not homogeneous under the chain and is greatest in the central part associated with the NW–SE depression. The estimated Moho geometry is in good agreement with refraction seismic data, which indicate a Moho deepening under the Central System (ILHA, 1993). A WNW–ESE refraction seismic model applied across the western-central region of the chain (Salamanca-Toledo, Fig. 9) reveals a Moho at a depth of 34 km, 1 km deeper than our results for the same area (Suriñach and Vegas, 1988).

To investigate the density structure of the crust, three gravity profiles were modelled.

Table 1

Density values for the different crustal units defined by the seismic models according to the relationship between P-wave velocity and density (Christensen and Mooney, 1995)

P-wave velocity (m/s)	Density (kg/m <sup>3</sup> )	
2000–4500	2000–2490	Sedimentary cover
5500–6000	2650–2710	Basement
6000–6800	2710–2860	Middle crust
6800–7100	2860–2960	Lower crust
8200	3300	Mantle

## 8. Gravity modelling

Two density models transverse to the Central System and a further model running parallel to this chain were constructed (Fig. 10A). Refraction seismic data were used as the starting point to constrain the deep structure. Thus, according to the seismic data the crust consists of three layers: (1) an upper 11 km thick crust, (2) a middle 11 km thick crust and (3) a lower 9 km thick crust (Fig. 1B, see Section 2). Isopach maps of the sedimentary basins derived from reflection seismic profiling were used to establish the geometry of the basins in the density models (see Section 4.1). In addition, geological mapping boundaries mapped at the surface and structural data were used to constrain upper crust density structure. From these constraints, initial models were developed. The modelling process was undertaken in 2D using the software GM-SYS 4.7 for Windows (2001).

As density constitutes a fundamental parameter in gravity modelling, measurements of density were derived from both field samples and well data. The field samples collected were 101 rock specimens with the most representative lithologies of the study area, including Variscan basement metamorphic and igneous rocks and Mesozoic and Cenozoic sedimentary rocks (Fig. 10). Neogene sediment density was mainly estimated from density-log data obtained from wells (see Section 4.1) and crustal layers densities from the P-wave velocity–density relationship (see Table 1).

Table 2 summarises the density bodies of models and corresponding crustal blocks.

Gravity anomalies of the transverse models, models 1 and 2 (Fig. 11), ranged from  $-70$  to  $-115$  mGal. The Bouguer anomaly pattern shows a central gravity high bounded by NW and SE gravity lows. Initial models showed reasonable fitting of the gravity data based on the densities outlined in Table 2. Combined basin infilling and crust thickening gravity effects fit the gravity lows. Middle crust thickening is required to fit the gravity high. The base of the middle crust deepens according to lower crust geometry, and the base of the upper crust rises up to 4 km. Crust structure is a block elevated at the faults of the NW and SE borders of the Central System. Modelling suggests fault dips close to 50°. Most of the shorter wavelength anomalies coincide with outcropping structures. Measured densities and geological map-



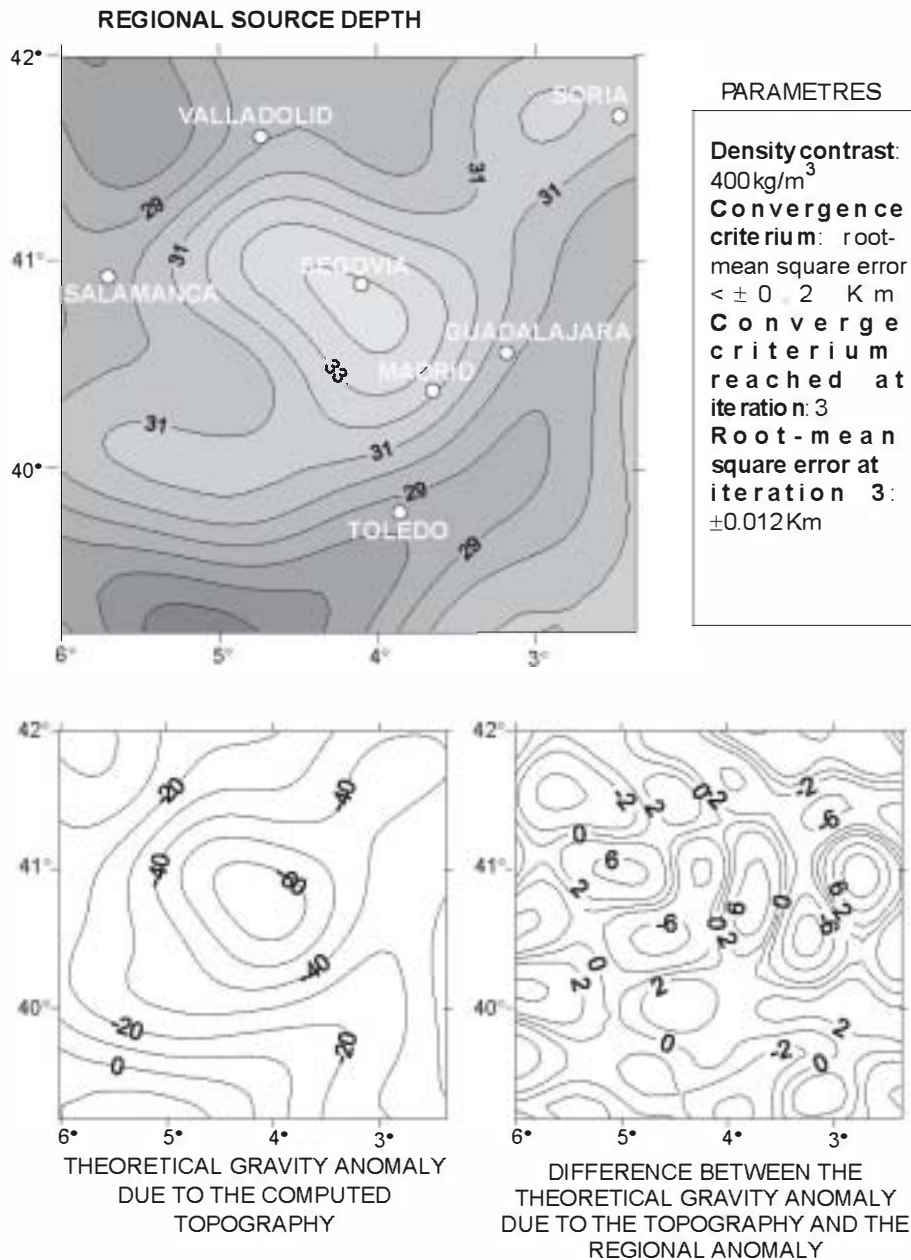


Fig. 9. Moho depth map of Central Spain obtained by applying the inversion method of [Jödenburg \(1974\)](#) to the regional gravity map in [Fig. 8A](#). Contour interval 1 km. Geographical coordinates. The lower figure shows the computed anomaly due to the Moho topography obtained, and the difference between this map and the regional gravity map used in the inversion procedure.

ping constrained density body geometries that were progressively refined to fit the anomalies. To achieve good anomaly fit in model 2, a new body of density 2720 kg/m<sup>3</sup> had to be introduced under the northern

border of the Tajo Basin (km 140 to 160). Both models show a heterogeneous upper crust. Anomaly fitting requires the existence of bodies of different densities corresponding to the Variscan basement.

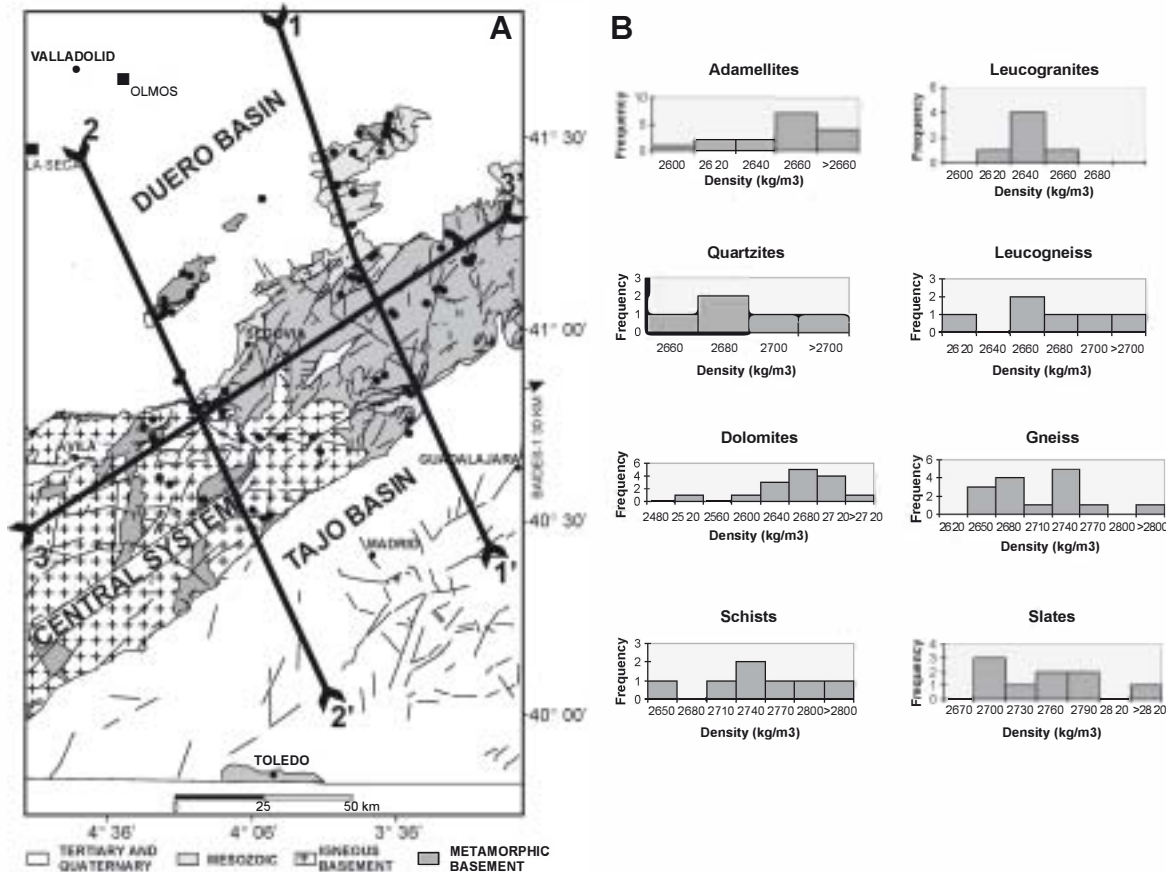


Fig. 10.

logs (black squares). Also shown is the location of the gravity models described in the text.

Beneath sedimentary basins, the basement comprises bodies of density  $2780 \text{ kg/m}^3$ . According to geological data, these correspond to sequences of low-grade metamorphic rocks, mainly slates and quartzites. In the Central System less dense materials predominate, corresponding to outcrops of high grade metamorphic rocks and granite.

The most interesting feature of model 3 (Fig. 11) is the clear density heterogeneity in the upper crust. The observed gravity anomaly shows a very simple geometry, corresponding to a gravity low of long wavelength, starting at values of  $-80 \text{ mGal}$  and reaching up to  $-95 \text{ mGal}$  at the centre of the profile. Although crust thickening and the resulting Moho deepening fitted the regional anomaly trend, to achieve good fit, we considered lateral density variation within the upper crust. A density body some 6

km thick of density  $2660 \text{ kg/m}^3$  characterizes the western upper crust. In the central part, a body of density  $2680 \text{ kg/m}^3$  and thickness 9 km is required to fit the anomaly. In the eastern area, a maximum depth of 11 km is reached and the body has a density of  $2720 \text{ kg/m}^3$ .

These findings indicate three domains with different predominant lithologies comprising the uppermost part of the crust, and different bodies corresponding to granite intrusions of density values  $2620 \text{ kg/m}^3$  and  $2650 \text{ kg/m}^3$  distributed over the area. The easternmost end of the model shows a more complex geometry, with several bodies increasing in density towards the east limited by shear zones. A Variscan normal detachment fault called the Berzosa-Riaza shear zone places low-grade metamorphic rocks (higher density rocks) over high-grade

Table 2  
Mean density values used in the gravity modelling

Unit		Density (kg/m <sup>3</sup> )
Mesozoic Cover	Neogene (lutites and sandstones)	2150
	Palaeogene (gypsum, sandstones, lutites, conglomerates)	2400
	Cretaceous (62.5% dolomites, 37.5% sandstones)	2650
	Jurassic (limestones)	2710
	Triassic	2650
Variscan Basement	Leucogranites	2620
	Adamellites	2660
	Leucogneisses	2720
	Gneiss	2680
	Slates	2780
	Quartzites	2680
	Schists	2740
Middle crust		2800
Lower crust		2900
Mantle		3300

gneissic complexes (lower density rocks) (e.g., Escuder Viruete et al., 1998).

## 9. Discussion

Gravity data analysis and gravity modelling were used to construct a crustal density model of the central Iberian Peninsula. Crustal thickening in the area includes an increased middle crust thickness under the Central System reaching the Moho at a depth below 34 km. These findings are consistent with the seismic model of the crust, although the depth of the Moho established by spectral analysis is slightly lower. This discrepancy could be due to discrete lateral variation in the density contrast at the lower crust–mantle boundary, as has been pointed out by other authors for similar areas (e.g., Lefort and Agarwal, 2002).

Lateral density variations along the length of the Central System characterize the upper crust, in which three density domains are distinguished by the density models. From east to west, density and the thickness of the upper crust decrease (Fig. 11, model 3). In the eastern region, the Variscan basement is represented by two bodies of densities 2780 kg/m<sup>3</sup> and 2680 kg/m<sup>3</sup> bounded by a regional structure, the N–S trending Berzosa-Riaza shear zone, which corresponds to an

east-dipping shear zone active in Variscan and Late-Variscan deformation events (e.g., Escuder Viruete et al., 1998). To the west, the basement is comprised of a body of density 2660 kg/m<sup>3</sup> corresponding at the surface to the granite outcrops that dominate the area. At first sight, the limit between this body and that of density 2680 kg/m<sup>3</sup> does not appear to coincide with a main mapped structure such as the Berzosa shear zone, but in the area, mylonites associated with deep ductile Variscan thrusts outcrop (Macaya et al., 1991). The Variscan basement of the central and western part of the Central System are dominated by high to medium metamorphic grade rocks while in the eastern zone underlying adjacent sedimentary basins, rocks of low metamorphic grade and higher densities predominate. Density variations appear to be an inherited feature of Variscan and Late-Variscan tectonic events.

As observed in the transverse density models, the Central System comprises an upper crust uplifted-block bounded by reverse faults. The upper crust uplifts to 4 km. This value matches the vertical displacement estimated taking into account the topographic elevation (~maximum 2.6 km) and the depth at the top of the Variscan basement beneath the basins (~maximum 2.5 km below sea level). The Central System structure is the result of compressive deformation events during the Alpine orogeny. Several explanations for crust thickening have been proposed. Some suggest that the Central System arose from block rotation and distributed deformation accompanied by ductile thickening in the middle and lower crust (Vegas et al., 1990). Other explanations have been based on a thrust tectonic model (Warburton and Alvarez, 1989; Ribeiro et al., 1990; Tejero et al., 1996). Any explanation for Central System formation must account for NE–SW compressive structures and crust thickening. We propose a NW-directed crustal thrust that could be rooted at the Moho (Fig. 12). This thrust would split into several high-angle reverse faults verging both NW and SE. The north border fault is the expression of this thrust at the surface. The south border fault represents a back-thrust. Thrust ramp and flat geometry will depend on the crust's mechanical structure. Present rheological stratification shows that ductile behaviour prevails at depths greater than 18 km (Tejero and Ruiz, 2002). Assuming a similar rheological structure, frontal and

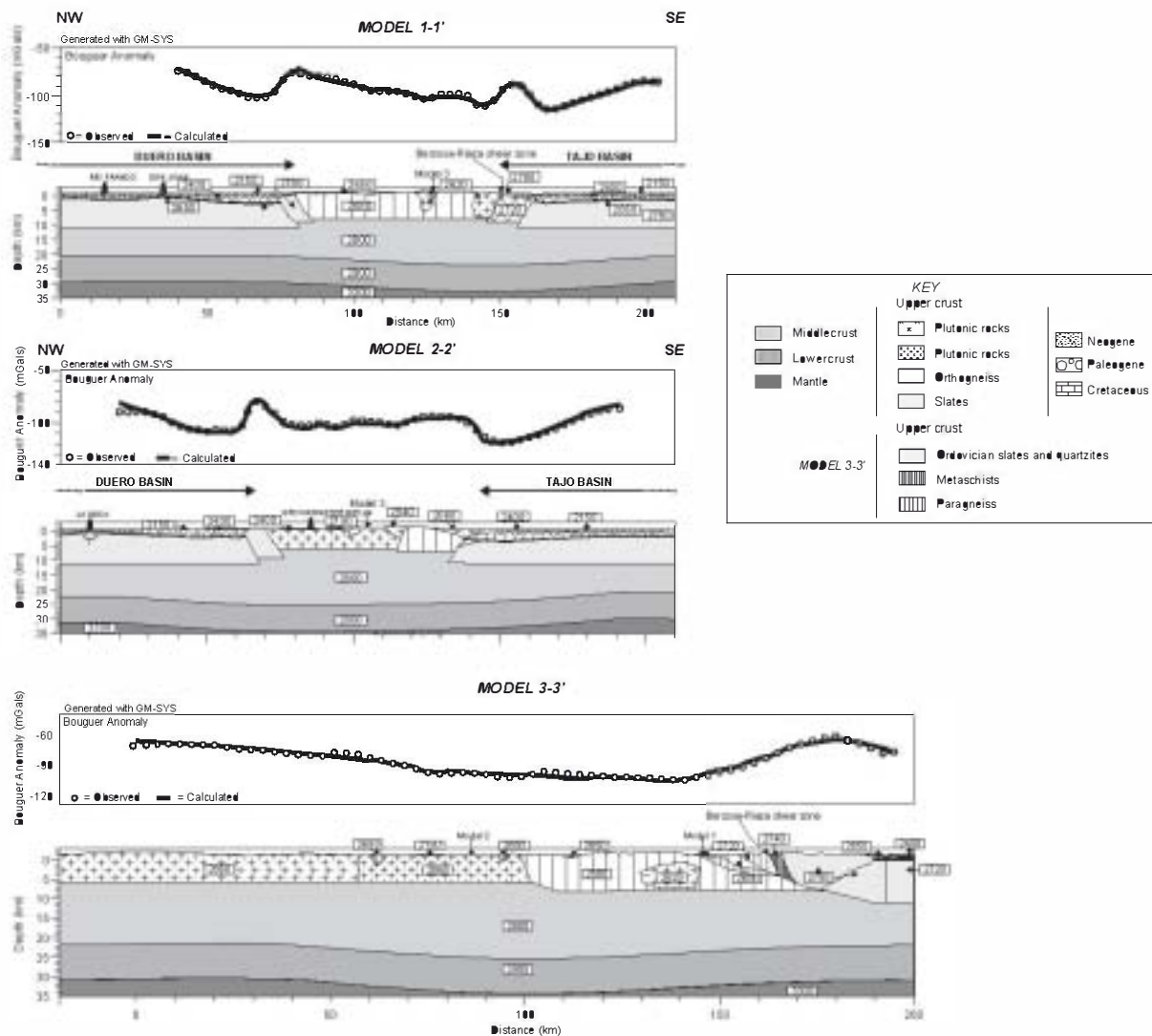


Fig. 11. 2 + 1/2 D gravity models constructed for the study area. For each model (from top to bottom), the gravity anomaly and the density model are represented. The three main crustal layers correspond to the refraction seismic model shown in Fig. 1B. See text for a description and further details.

back thrusts would be linked at depth by a flat ductile detachment lying within the weak zone of the middle crust. Thrust emplacement would explain the thickening of the middle crust. Through spectral analysis, the maximum depth of the Moho is located in the central part of the chain. In this area, basin depocentres occur close to the Central System border related to higher values of basin subsidence and chain uplift. This could be linked to a maximum thrusting displacement in this region.

## 10. Conclusions

Based on the analysis and modelling of gravity data constrained by geological and seismic information, we constructed a model of crust structure for the central region of the Iberian Peninsula.

- Subtraction of the expected long-wavelength Bouguer anomaly due to basin sedimentary infill from the observed Bouguer anomaly provides a



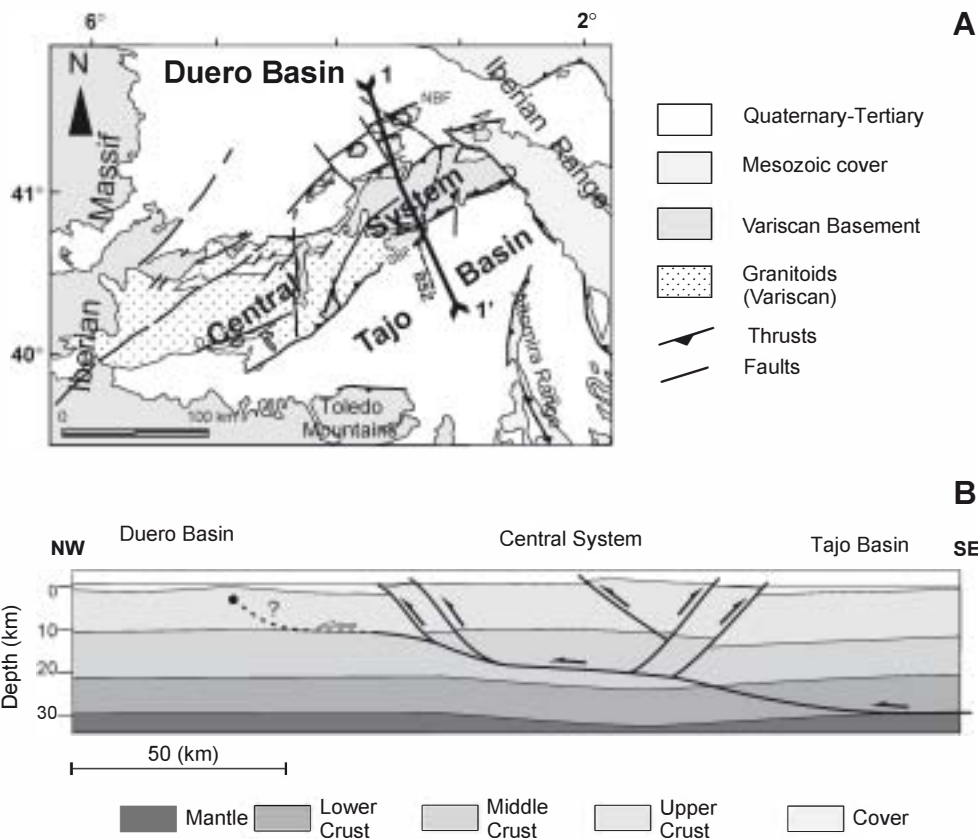


Fig. 12.

- Bouguer anomaly data set caused by the structures below the basins, mainly deep-seated sources.
- Subsequent energy spectrum analysis of this data set reveals the existence of two distinct linear segments. The slope of the shallowest depth segment ( $11 \pm 0.2$  km) corresponds to the mean depth of the upper crust base and the depth given by the steepest slope ( $31.1 \pm 3.6$  km) corresponds to the mean Moho depth.
- A NE–SW depression characterizes Moho topography. The Moho deepens to up to 34 km under the Central System.
- A gravity model parallel to the Central System and transverse to the Variscan structure indicates several density domains that represent different tectonic domains bounded by a Variscan ductile crustal shear zone.

- Gravity models transverse to the chain suggest its structure consists of an 80 km wide crustal block uplifted by reverse NE–SW to E–W faults. The middle crust appears thickened in the Central System.
- Crust structure is the result of Variscan and Alpine deformations. Variscan structures limit different density bodies within the basement. The overall structure of the Central System is Alpine. It consists of an uplifted crustal block. Displacement occurs along a NW-directed middle crust thrust, probably rooted at the Moho.

The Bouguer gravity field of the central Iberian Peninsula reflects the combined effects of an inherited Variscan structure and Mesozoic tectonic events. While crustal thickening is related to an Alpine chain formation—the Central System—lateral density

variations seem to be associated to Variscan basement structure.

## Acknowledgements

This research was supported by the Project BTE-2003-03902 (Ministerio de Educación y Ciencia, Spain). We wish to thank Dr. Garcia-Abdeslem, an anonymous reviewer and the Editor for their constructive comments on the manuscript. We also thank Ana Burton for linguistic assistance.

## References

- Aeroservice Ltd., 1967. Mapa geológico de la Cuenca del Duero. Escala 1:250.000. Inst. de Colonización e Inst. Geológico y Minero de España. Madrid.
- Banda, E., Suriñach, E., Aparicio, A., Sierra, J., Ruiz de la Parte, E., 1981. Crust and upper mantle structure of the central Iberian Meseta (Spain). *Geophys. J. R. Astron. Soc.* 67, 779–789.
- Blanco, J., Merten, R., 1974. Mapa de isobatas para el techo del Paleozoico y base del Terciario en la Cuenca del Duero. Hispanoil.
- Bond, J., 1996. Tectono-sedimentary evolution of the Almazan Basin, NE Spain. In: Friend, F., Dabrio, C.J. (Eds.), *Tertiary Basins of Spain: The Stratigraphic Record of Crustal Kinematics*. Cambridge University Press, Cambridge, Great Britain, pp. 203–213.
- Bott, M.H.P., 1960. The use of rapid digital computing methods for direct gravity interpretation of sedimentary basins. *Geophys. J. R. Astron. Soc.* 3 (1), 63–67.
- Capote, R., De Vicente, G., González Casado, J.M., 1990. Evolución de las deformaciones alpinas en el Sistema Central. *Geogaceta* 7, 20–22.
- Chai, Y., Hinze, W.J., 1988. Gravity inversion of an interface above which the density contrast varies exponentially with depth. *Geophysics* 53 (6), 837–845.
- Chakraborty, K., Agarwal, B.N.P., 1992. Mapping of crustal discontinuities by wavelength filtering of the gravity field. *Geophys. Prospect.* 41, 801–822.
- Chakravarthi, V., Rao, C.V., 1993. Parabolic density function in sedimentary basin modeling. *Proceedings of the Eighteenth Annual Convention and Seminar on Exploration Geophysics*, Jaipur, India. p. A.16.
- Chakravarthi, V., Raghuram, H.M., Singh, S.B., 2002. 3-D forward gravity modeling of basement interfaces above which the density contrast varies continuously with depth. *Comput. Geosci.* 28, 53–57.
- Christensen, N.I., Mooney, W.D., 1995. Seismic velocity structure and composition of the continental crust: a global view. *J. Geophys. Res.* 100 (B7), 9761–9788.
- Cordell, L., 1973. Gravity analysis using an exponential density–depth function—San Jacinto Graben, California. *Geophysics* 38 (4), 684–690.
- De Vicente, G., González Casado, J.M., Muñoz, A., Giner, J., Rodríguez Pascua, M.A., 1996a. Structure and tertiary evolution of the Madrid Basin. In: Friend, F., Dabrio, C.J. (Eds.), *Tertiary Basins of Spain: The Stratigraphic Record of Crustal Kinematics*. Cambridge University Press, Cambridge, Great Britain, pp. 263–267.
- De Vicente, G., Giner, J., Muñoz, A., González-Casado, J.M., Lindo, R., 1996b. Determination of present-day stress tensor and neotectonic interval in the Spanish Central System and Madrid Basin, central Spain. *Tectonophysics* 266 (1–4), 405–424.
- Dimitriadis, K., Tselentis, G.A., Thanassoulas, K., 1987. A basic program for 2-D spectral analysis of gravity data and source-depth estimation. *Comput. Geosci.* 13 (5), 549–560.
- Escuder Viruete, J., Hernáiz Huerta, P.P., Valverde Vaquero, P., Rodríguez Fernández, R., Dunning, G., 1998. Variscan syn collisional extension in the Iberian Massif: structural, metamorphic and geochronological evidence from the Somosierra sector of the Sierra de Guadarrama (Central Iberian Zone, Spain). *Tectonophysics* 290 (1–2), 87–109.
- GM-SYS v. 4.7, 2001. Gravity/Magnetic Modeling Software. Northwest Geophysical Associates, Inc., P.O. Box 1063, Corvallis, OR 97339, USA.
- Gómez Ortiz, D., 2001. La estructura de la corteza en la zona central de la Península Ibérica. PhD thesis, University Complutense de Madrid, Madrid.
- Granser, H., 1987. Three-dimensional interpretation of gravity data from sedimentary basins using an exponential density–depth function. *Geophys. Prospect.* 35 (9), 1030–1041.
- Gupta, V.K., Ramani, N., 1980. Some aspects of regional-residual separation of gravity anomalies in a precambrian terrain. *Geophysics* 45 (9), 1412–1426.
- I.G.M.E., 1987. Contribución de la exploración petrolífera al conocimiento de la geología de España. IGME, Madrid. 465 pp.
- ILHA DSS Group, 1993. A deep seismic sounding investigation of lithospheric heterogeneity and anisotropy beneath the Iberian Peninsula. *Tectonophysics* 221 (1), 35–51.
- I.T.G.E., 1990. Documentación sobre la geología del subsuelo de España. Tomo V (Duero-Almazán). Internal report number 29040, Madrid.
- Lees, J.M., Park, J., 1995. Multiple-taper spectral analysis: a stand-alone C-subroutine. *Comput. Geosci.* 21, 199–236.
- Lefort, J.P., Agarwal, B.N.P., 2002. Topography of the Moho undulations in France from gravity data: their age and origin. *Tectonophysics* 350, 193–213.
- Macaya, J., González-Loecheiro, F., Martínez-Catalán, J.R., Alvarez, F., 1991. Continuous deformation, ductile thrusting and backfolding of cover and basement in the Sierra de Guadarrama, Hercynian orogen of central Spain. *Tectonophysics* 191, 291–309.
- Maestro, A., 1999. Estructura y evolución alpina de la Cuenca de Almazán (Corallera Ibérica). PhD thesis. University of Zaragoza, Zaragoza.

- Martin-Atienza, B., Garcia-Abdeslem, J., 1999. 2-D Gravity modeling with analytically defined geometry and quadratic polynomial density functions. *Geophysics* 64 (6), 1703–1734.
- Mezcua, J., Gil, A., Benarroch, R., 1996. Estudio Gravimétrico de la Península Ibérica y Baleares. Inst. Geográfico Nacional, Madrid. 7 pp.
- Mishra, D.C., Naidu, P.S., 1974. Two-dimensional power spectral analysis of aeromagnetic fields. *Geophys. Prospect.* 22, 345–353.
- Muñoz Martin, A., 1997. Evolución geodinámica del borde oriental de la Cuenca del Tajo desde el Oligoceno hasta la Actualidad. PhD thesis, University Complutense de Madrid, Madrid.
- Oldenburg, D.W., 1974. The inversion and interpretation of gravity anomalies. *Geophysics* 39 (4), 526–536.
- Parker, R.L., 1973. The rapid calculation of potential anomalies. *Geophys. J. R. Astron. Soc.* 31, 447–455.
- Querol, R., 1989. Geología del subsuelo de la Cuenca del Tajo. ITGE-ETSI de Minas de Madrid, Madrid. 48 pp.
- Rey Moral, C., 2001. Estudio geofísico de una cuenca sedimentaria: La Cuenca de Almazán (provincia de Soria). Implicaciones tectónicas. PhD thesis. University Complutense de Madrid, Madrid.
- Ribeiro, A., Kullberg, M.C., Kullberg, J.C., Manuppella, G., Phipps, S., 1990. A review of Alpine tectonics in Portugal: foreland detachment in basement and cover rocks. *Tectonophysics* 184 (3–4), 357–366.
- SHELL, 1983. Informe del sondeo Baidés-1. Internal report.
- Slepian, D., 1978. Prolate spheroidal wave functions, Fourier analysis and uncertainty, V, the discrete case. *Bell Syst. Tech. J.* 57, 1371–1429.
- Spector, A., Grant, F.S., 1970. Statistical models for interpreting aeromagnetic data. *Geophysics* 35 (2), 293–302.
- Surinach, E., Vegas, R., 1988. Lateral inhomogeneities of the Hercynian crust in central Spain. *Phys. Earth Planet. Inter.* 51, 226–234.
- Syberg, F.J.R., 1972. A Fourier method for the regional-residual problem of potential fields. *Geophys. Prospect.* 20, 47–75.
- Tejero, R.M., Ruiz, J., 2002. Thermal and mechanical structure of the central Iberian Peninsula lithosphere. *Tectonophysics* 350, 49–62.
- Tejero, R., Perucha, M.A., Rivas, A., Bergamín, J.F., 1996. Modelos gravimétrico y estructural del Sistema Central. *Geogaceta* 20 (4), 947–950.
- Tselentis, G.A., Drakopoulos, J., Dimitriadis, K., 1988. A spectral approach to Moho depths estimation from gravity measurements in Epirus (NW Greece). *J. Phys. Earth* 36, 255–266.
- Vegas, R., Vázquez, J.T., Surinach, E., Marcos, A., 1990. Model of distributed deformation, block rotations and crustal thickening for the formation of the Spanish Central System. *Tectonophysics* 184, 376–378.
- Warburton, J., Alvarez, C., 1989. A thrust tectonic interpretation of the Guadarrama Mountains, Spanish Central System. Libro Homenaje a Rafael Soler. Asoc. Geol. Geof. Esp. del Petróleo (AGGEP), pp. 147–155.